LA-9195-MS

UC-38
Issued: March 1982

LA--9195-MS

DE82 014129

Calibration of an Electron/Proton Monitor for the Earth's Radiation Belt at 4 R_E

Paul R. Higbie
Richard D. Belian
Harold V. Argo
Daniel N. Baker

Los Alamos National Laboratory
Los Alamos, New Mexico 87545

CALIBRATION OF AN ELECTRON/PROTON MONITOR FOR THE EARTH'S RADIATION BELT AT 4 R_E

by

Paul R. Higbie, Richard D. Belian, Harold V. Argo, and Daniel N. Baker

ABSTRACT

A charged particle dosimeter (the Burst Detector Dosimeter or BDD) was designed and fabricated and will be flown on certain of the Global Positioning Satellite (GPS) series of spacecraft. The BDD will monitor the dose received by the GPS spacecraft from the fluxes of electrons and protons in the Earth's radiation belt. The BDD uses absorbers in front of silicon sensors to determine the energy thresholds for measuring incident particle fluxes; and the magnitude of energy loss in a single sensor distinguishes between ions and electrons over a wide range of energies. Our electron calibrations were performed to determine accurately the energy response function of the dosimeter. The experimentally determined energy and angular responses are used to determine the equivalent energy thresholds and geometric factors for idealized step function responses.

INTRODUCTION

Because of existing GPS system constraints, requirements, and time pressure, we decided to use a simple absorber type of design for the BDD instead of a more sophisticated design, such as a telescope arrangement of sensors or a magnetic spectrometer. An absorber design, however, does not provide as clear a particle identification nor as precise an energy measurement as the other designs. The immediate consequence then is a need to calibrate the detectors accurately to interpret on-orbit data. The basic design of the BDD system was discussed in detail by Argo,[1] but we provide a brief introductory description here and then detail the physical calibration of a BDD unit.

The BDD consists of four 700-μm-thick semiconductor sensors, each covered by thick graded shields or "domes" that reduce to acceptable levels the flux reaching the sensor elements from directions not occulted by the spacecraft body. The shields consist of aluminum and gold hemispheres into which are

Fig. 1 The BDD instrument showing the thick shields, or domes. The multiple holes provide a uniform sampling of 2π steradians. An inner thin hemispheric absorber lies at the base of the holes.

drilled either 13 or 14 holes to sample uniformly the available 2π steradians (Fig. 1). An inner thin-shelled hemisphere within each dome provides an absorber at the bottom of each hole. Table I provides a list of the pertinent parameters for these shields. Two electronic thresholds on the output signal from the solid state semiconductor sensors distinguish electrons from protons. Each electron channel responds to (1) protons that just penetrate the domes or absorbers and have a small residual energy, and (2) very energetic protons; but the contribution of such background effects to the total electron counting rate is expected to be small.

An analog-to-digital converter (ADC) measures and converts to a digital count the energy lost by a particle incident on each BDD semiconductor sensor. The output pulses from the ADC are prescaled so that one output pulse is equivalent to 2 MeV lost in the sensor. Thus, eight minimum ionizing electrons, each losing approximately 250 keV, would generate a single output pulse. The BDD uses a 2-MHz clock (4 MHz on later models to reduce dead time) with a conversion gain such that the ADC requires 160 μs to convert a 10-MeV

TABLE I

DETECTOR CHARACTERISTICS

Outer radius of domes, 1.77 cm
Inner radius, 0.64 cm
Graded shield material: inner - gold
outer - aluminum

Electronic Channel	Hole Diameter (mm)	Number of Holes	Filter Material	Filter Thickness (mm)	Thickness of Inner Shield (mm)
1	1.506	13	Al	0.23	5.1
2	1.984	14	Fe	0.53	1.9
3	1.613	13	Al	0.61	3.2
4	2.705	14	W	0.38	0.64

pulse. This corresponds to the maximum energy loss that can be deposited by protons stopping in the sensor.

The relationship between the counting rate and the response function for a given channel can be written as

$$CR = \int_0^\infty dE \sum_i \int_{\Omega_i} R(E)\, \eta(\theta,E)\, N(E,\gamma)\, d\Omega \quad , \tag{1}$$

where $R(E)$ is the energy response of the instrument for a monoenergetic beam directed along the central axis of one of the holes, $\eta(\theta,E)$ is the normalized response of the hole ($\eta(0) = 1$), the summation over i represents the contribution of all holes in the shield, and $N(E,\gamma)$ is the energy spectrum of incident particles, the shape of which is parameterized by the single variable γ. $N(E,\gamma)$ is assumed to be isotropic. Now, if we had an ideal sensor with a step function response we could write

$$CR = R^* \int_{4\pi} \int_{E^*}^\infty N(E,\gamma)\, E\, dE\, d\Omega \quad , \tag{2}$$

where E^* is the effective energy threshold and R^* takes into account the aperture of the instrument.

Letting $N = N_0 G(E,\gamma)$ and equating (1) and (2), we have a relation between R^*, E^*, and γ which is independent of the magnitude of the spectrum, N_0, but does depend on the measured quantities $R(E)$ and $\eta(\theta,E)$, i.e. $R^* = R^*(E^*,\gamma)$. A later section gives a choice for R^* and E^*, which minimizes the dependence on γ. For this choice the integral spectrum[1] folded with the energy will be given by

$$\langle E\, N(>E^*)\rangle = \int_{E^*}^\infty E\, N(E,\gamma)\, dE = CR/4\pi R^* \quad . \tag{3}$$

Electrons can undergo a variety of processes as they interact with matter in the collimating holes of the sensor shields or as they pass through the absorbers at the bottoms of the shields.

LOWER ENERGY RANGE CALIBRATION

Calibrations were performed at Aerospace for energies from 200 keV to 2.5 MeV. A magnetic spectrometer was used with a ^{106}Ru source placed at one focal point and the BDD near the other. The magnetic-field/energy relationship was determined by measuring the total energy loss peak in a 2-mm-thick semiconductor sensor as a function of energy. Repeatability of measurements was better than 50 keV. The beta spectrum of the ^{106}Ru source measured by the monitor sensor gave the counting rate curve shown in Figure 2. The end-point energy of the source is 3.4 MeV, but we were limited to approximately 2.5 MeV during calibrations because beyond this point the counting rate varies rapidly with energy.

The BDD instrument and the monitor sensor were both mounted on a rotating table inside a large vacuum chamber. The monitor sensor was covered by a 0.15-in.-thick lead shield that had a 0.152-in. - aperture hole in it. The system was carefully aligned with a laser so that the monitor could be rotated onto the central axis of the spectrometer at the point previously occupied by the BDD channel being measured. The mounting bracket for the BDD was designed so that the central hole for any of the four channels could be located along the central axis. To maximize the counting rate, the system was run fully open, with the aperture defined by the geometry of the bending magnet assembly. The relative counting rate between the monitor sensor and the BDD was used to define the shape of the energy response curves with good precision. After the completion of these runs, the monitor and the BDD domes were successively located at the focal point and the magnetic spectrometer's exit aperture was defined by a 1/2-in.-thick plate of lucite with a 1/4-in.-diam hole. The angular divergence of the beam was then less than the half angle of any of the dome holes or the monitor aperture. The threshold on the monitor was set at 100 keV so that it would detect all incident electrons. Thus an absolute calibration point could be obtained for each channel. The angular response for one of the channels (Channel 3) was also obtained under these conditions and

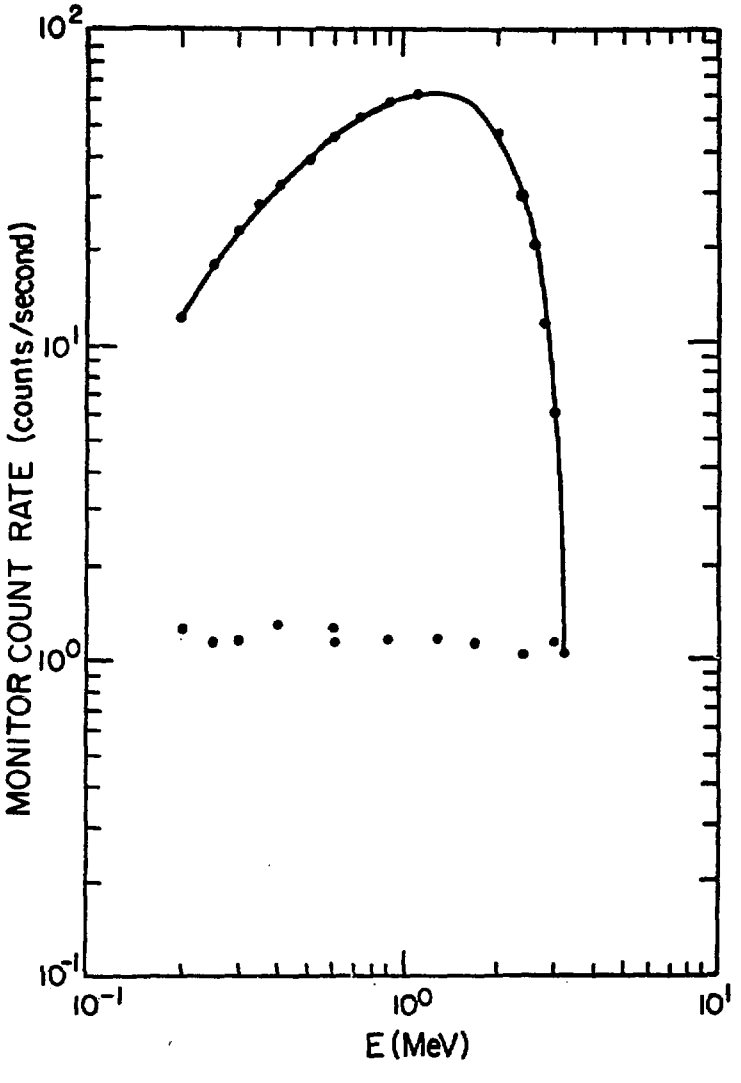

Fig. 2 Monitor counting rate curve for the ^{106}Ru source used in the magnetic spectrometer calibration at Aerospace. The rapid change in rate for energies close to the end point limits the useful portion of the spectum to 2.5 MeV.

confirmed that the optical alignment coincided well with the central ray through the spectrometer and exit aperture.

The results of the calibration at the Aerospace facility are given in Table IIa. The relative response R is given by the relation

$$R = (BDD-BKG)/MONITOR \quad ,$$

where BDD is counts per accumulation period (3.2 min), BKG is background counts per accumulation, and MONITOR corresponds to number of monitor counts per second.

Table IIb presents the results of the one-point absolute calibrations described above. The normalization factors derived from these points have been used to calculate the normalized responses given in Table IIa and illustrated in Fig. 3.

The angular response curve for Channel 3 was measured in detail. The table axis was positioned at the entrance aperture for the central hole in the dome, and the table was stepped in azimuth for several measurements. The results are illustrated in Fig. 4. The peak of the distribution was within approximately 0.5^{o} of the optically determined central axis. The angular response determined by a run at the electron accelerator at Sandia Laboratories is also shown for an energy of 750 keV.

Both curves indicate an opening angle greater than that determined from the calculated geometrical response of the hole.[2]

For two holes with equal radii, the response function is given by

$$R(\theta) = r^2 \cos\theta [2\psi - \sin 2\psi] \quad ,$$

TABLE IIa

CENTRAL HOLE CALIBRATIONS AT AEROSPACE

Channel 1			Channel 2			Channel 3			Channel 4		
E[a]	R[b]	N*R[c]	E[a]	R[b]	N*R[c]	E[a]	R[b]	N*R[c]	E	R	N*R
0.35	0.81	0.52	0.80	0.1	-	0.60	0.30	0.16	1.40	0.10	0.11
0.40	1.22	0.78	0.90	0.1	-	0.65	0.54	0.29	1.50	0.22	0.25
0.45	1.89	1.21	1.00	0.1	-	0.70	1.16	0.61	1.60	0.38	0.43
0.50	2.45	1.57	1.05	0.20	0.14	0.80	1.62	0.86	1.70	0.57	0.64
0.60	3.80	2.43	1.10	0.43	0.31	0.90	2.81	1.49	1.80	0.83	0.93
0.70	4.52	2.89	1.15	0.67	0.48	1.00	3.18	1.63	1.90	1.13	1.27
0.80	5.15	3.30	1.20	0.90	0.65	1.10	3.65	1.93	2.00	1.27	1.42
0.90	5.98	3.83	1.30	1.45	1.04	1.20	3.79	2.01	2.10	1.83	2.05
1.00	6.32	4.04	1.40	1.92	1.38	1.40	3.65	1.93	2.20	1.76	1.97
1.10	5.85	3.74	1.50	2.42	1.78	1.60	3.91	2.07	2.30	2.83	3.17
1.21	5.00	3.20	1.60	2.78	2.00	1.80	4.14	2.19	2.40	2.57	2.88
1.42	5.60	3.58	1.70	3.22	2.32	2.00	4.24	2.25	2.50	3.40	3.81
1.63	5.34	3.42	1.80	3.76	2.71	2.20	4.18	2.22	2.60	4.05	4.54
1.84	5.24	3.35	1.90	3.77	2.71	2.40	4.52	2.40	2.70	3.56	3.99
2.00	5.12	3.28	2.00	3.93	2.83				2.80	5.75	6.44
2.50	5.16	3.30	2.10	3.83	2.76				2.90	5.13	5.75
3.00	9.29	5.95	2.20	4.24	3.05						
			2.30	4.20	3.02						
			2.50	4.79	3.45						

[a]Energy (MeV)
[b]Relative response at 0^{o} incidence angle.
[c]Normalized response [counts/(el/cm^2)] x (10^{-3})

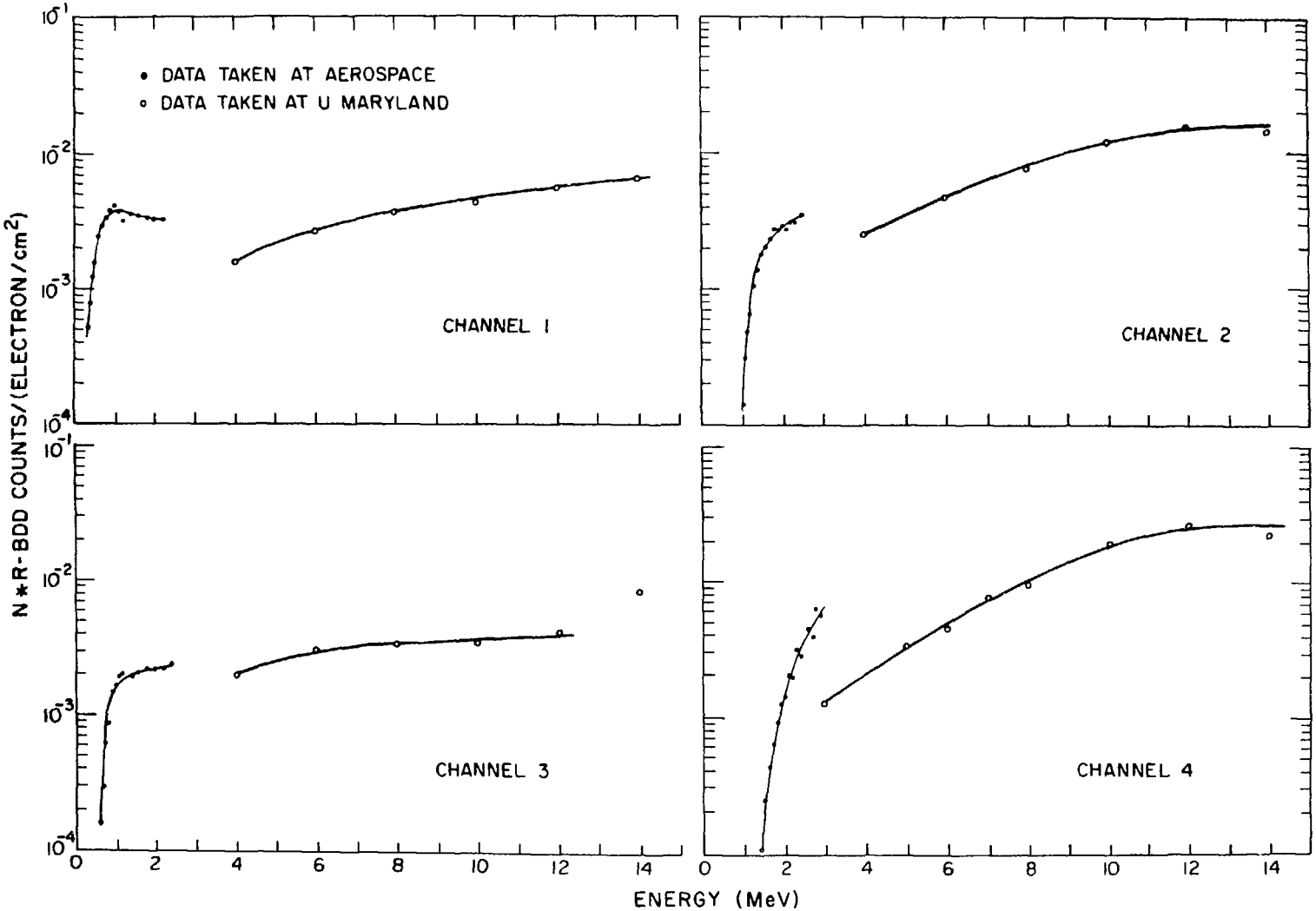

Fig. 3 Energy response of the four BDD channels for the central hole at normal incidence. Solid dots correspond to data taken at Aerospace; open circles to data taken at the University of Maryland.

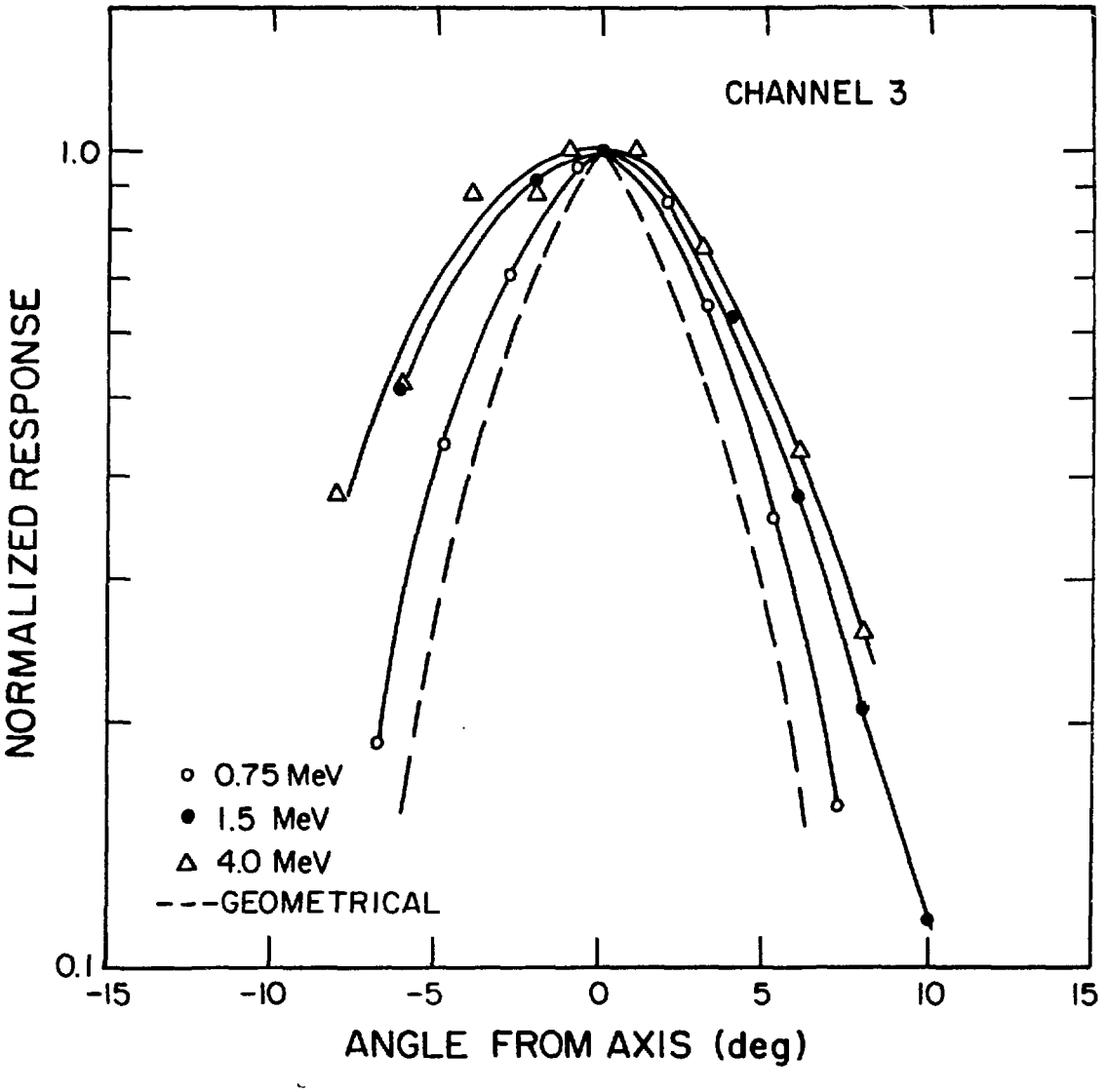

Fig. 4 Angular response function, $n(\theta)$, for Channel 3 at 0.75, 1.5, and 4 MeV; θ is the angle of rotation perpendicular to the laser-defined central axis through the entrance aperture of the central hole in the dome.

TABLE IIb

ABSOLUTE CALIBRATIONS AT AEROSPACE

Channel	E^{*a}	R^{*b}	N^{c}
1	2.0	3.34×10^{-3}	0.64×10^{-3}
2	2.0	2.82×10^{-3}	0.72×10^{-3}
3	1.5	2.07×10^{-3}	0.53×10^{-3}
4	2.0	1.45×10^{-3}	1.12×10^{-3}

[a]Energy of absolute calibration point (MeV)
[b]Absolute response at E^* [cts/(el/cm^2)]
[c]Normalization for Table Ia; $(R^*/R)|_{E^*}$

where r = the radius of the holes,

θ = the angle from normal incidence,

L = the distance between the holes,

and,

$$\psi = \cos^{-1}\left[\frac{L \tan\theta}{2r}\right] .$$

This response function is also shown in Fig. 4, and the half angles calculated from it are given in Table IV to be discussed later.

HIGHER ENERGY RANGE CALIBRATION

We used the University of Maryland's electron linear accelerator to calibrate the sensor at the higher energies. Figure 5 is a schematic view of the facility. The electron beam was bent upwards by the magnet A1 and passed through a concrete floor (indicated by the horizontal lines between the

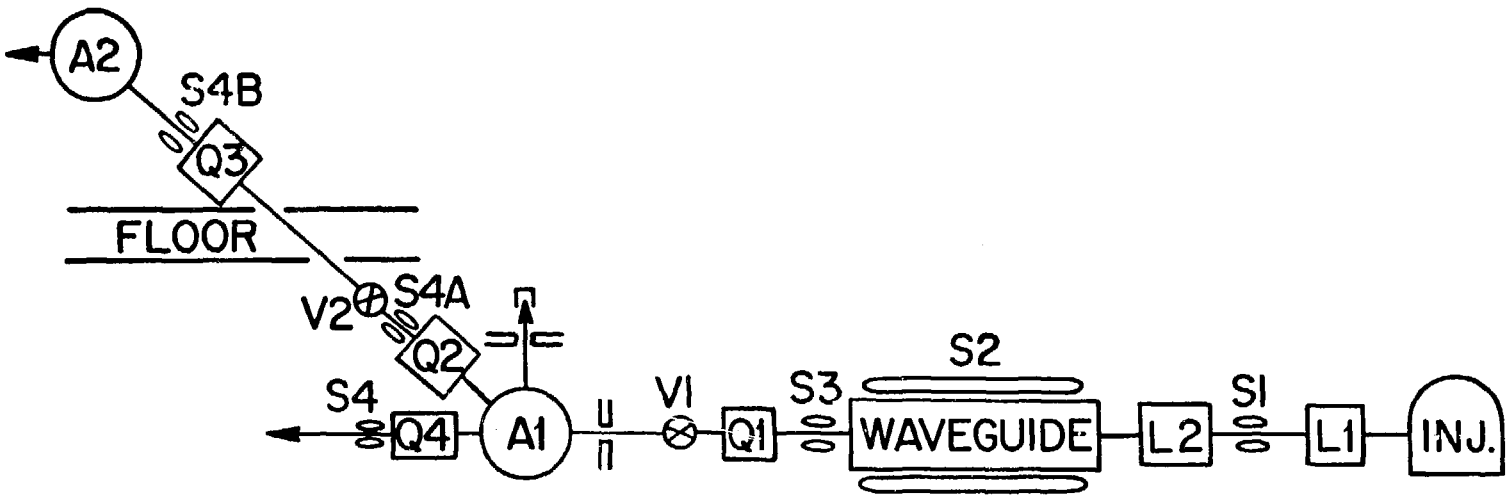

Fig. 5 Layout of the University of Maryland electron linear accelerator. See text for details.

quadrupole magnets Q2 and Q3). The beam was returned to the horizontal position by the bending magnet A2. From this point it entered the vacuum chamber, which contained a rotating table. The entire system was evacuated, and the beam aperture was defined by slits on the first floor to minimize scattering and background effects from bremsstrahlung.

The data from these calibrations are plotted as open circles on Fig. 3, and the raw data are also given in Table IIIa. The normalization was made by using the counting rate from a 0.5-cm^2 monitor sensor. It is apparent from comparison of the two sets of curves from the Aerospace and the University of Maryland data that some adjustments must be made in the normalization constants. This renormalization is discussed in a later section.

TABLE IIIa

CENTRAL HOLE CALIBRATIONS AT THE UNIVERSITY OF MARYLAND

Channel 1			Channel 2			Channel 3			Channel 4		
E	R^a	$N*R^b$	E	R^a	$N*R^b$	E	R^a	$N*R^b$	E	R^a	$N*R^b$
4.0	0.64	1.6	4.0	0.98	2.5	4.0	0.78	2.0	3.0	0.49	1.3
6.0	1.04	2.7	6.0	1.82	4.7	6.0	1.19	3.1	3.8	0.76	2.0
8.0	1.42	3.7	8.0	2.97	7.7	8.0	1.31	3.4	5.0	1.30	3.4
10.0	1.66	4.3	10.0	4.66	12.1	10.0	1.35	3.5	6.0	1.75	4.6
12.0	2.17	5.6	12.0	6.02	15.7	12.0	1.60	4.2	7.0	2.97	7.7
14.0	2.51	6.5	14.0	5.59	14.5	14.0	3.22	8.4	8.0	3.68	9.6
									10.0	7.36	19.1
									12.0	10.25	26.7
									14.0	8.59	22.3

[a]cts/sample
[b]Normalized response [cts/(el/cm^2)] x 10^{-3}; N = 2.6 x 10^{-3} cm^2/sec/sample.

ANGULAR DISTRIBUTIONS AT HIGHER ENERGIES

Angular response functions were measured for Channels 2, 3, and 4 at the arbitrarily chosen energies of 6, 4, and 3 MeV, respectively. The normalized responses for these measurements are given in Table IIIb. The response for Channel 3 has been added to Fig. 4. The response functions for Channels 2 and 4 are illustrated in Fig. 6. By interpolating the 80% point for the normalized

TABLE IIIb

NORMALIZED ANGULAR RESPONSE FROM UNIV. OF MARYLAND DATA

Channel 2 @ 6 MeV		Channel 3 @ 4 MeV		Channel 4 @ 3 MeV	
θ	n(θ)	θ	n(θ)	θ	n(θ)
0	1.0	-1	1.0	-2	0.9
-5	0.66	1	1.0	0	1.17
-10	0.41	3	0.76	2	0.9
5	0.80	5	0.43	4	1.1
		7	0.16	6	0.6
		-3	0.88	8	0.6
		-5	0.88	-2	1.1
		-7	0.52	-4	0.95
		-9	0.38	-6	0.6
				-8	0.4
				-10	0.3
				-12	0.2
				-14	0.3
				-16	0.3

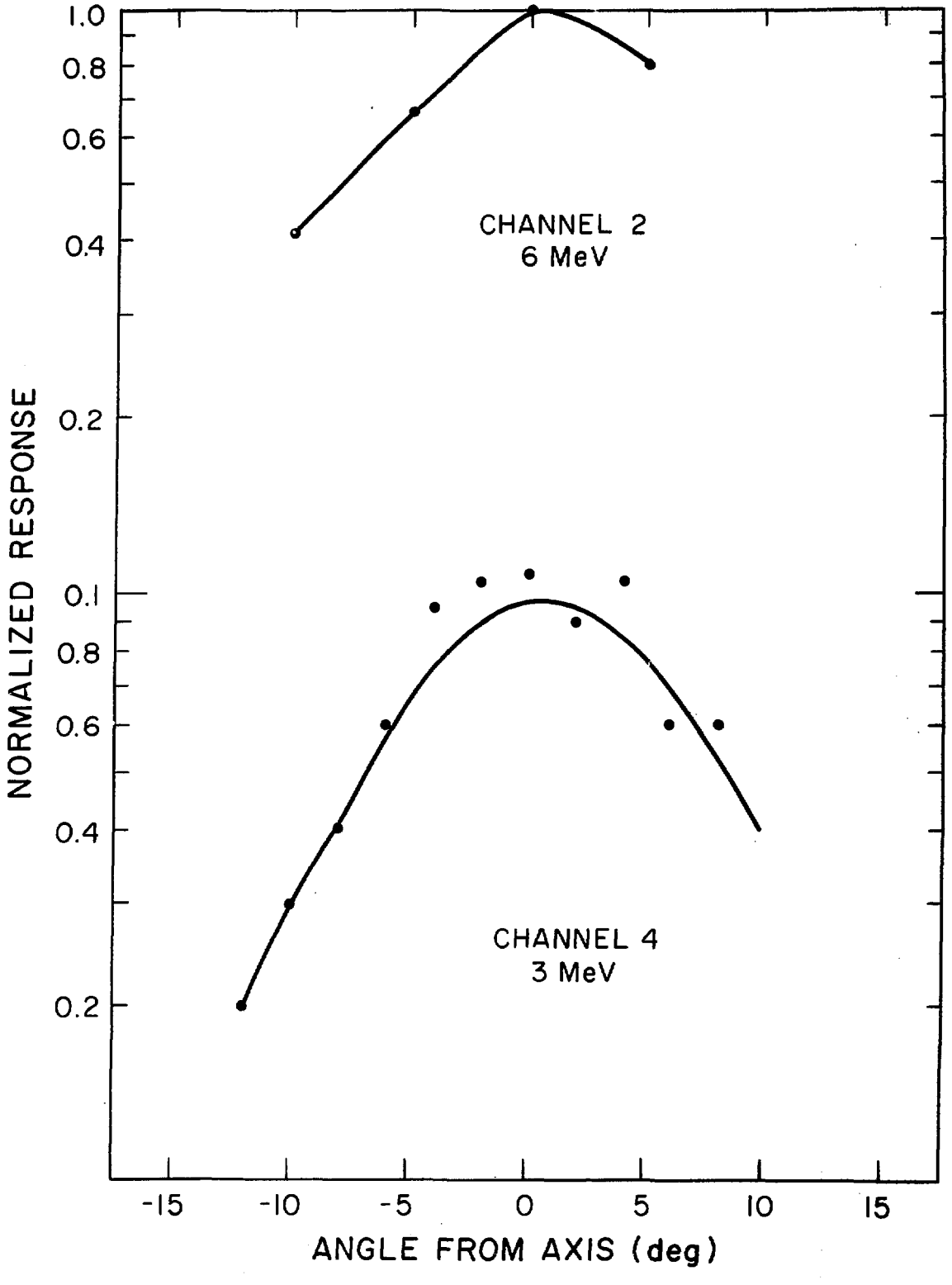

Fig. 6 Normalized angular response functions measured at the University of Maryland.

data for Channel 2 and by assuming a Gaussian form for the angular response function, a FWHM value of 10.8° was found for this channel.

PARAMETERIZATION OF THE ANGULAR RESPONSE ON ENERGY

Figure 4 shows that there is a clear energy dependence for the opening angles of the instruments. We assume that the distributions can be characterized by θ_{FWHM}. Furthermore, the effects of scattering, or transparency to energetic particles at the edges of the holes, are represented by θ_{SCATT}. The FWHM angle corresponding to purely geometrical effects can also be calculated.[2] We then assume that the effects of scattering are given by

$$\theta^2_{SCATT} = \theta^2_{FWHM} - \theta^2_{GEOM} .$$

In Fig. 7 these values are plotted as a function of the empirically selected parameter $\sqrt{E}$. A least squares fit to these points gives

$$\theta_{SCATT} = 5.27 \sqrt{E},$$

where E is in MeV and θ is in degrees.

The angular response is roughly Gaussian in shape, so that

$$\eta(\theta) = \exp -(\theta^2/.361\ \theta^2_{FWHM}) \quad ,$$

and $\theta^2_{FWHM} = \theta^2_{GEOM} + 27.8\ E$, where θ is measured from the hole axis. θ_{GEOM} is given in Table IV.

RENORMALIZATION OF THE ENERGY RESPONSE FUNCTION

As we pointed out above, the normalizations used to construct Fig. 3 do not give consistent results, albeit the curves correspond to putatively absolute calibrations. To match the slope and level of the curves based on

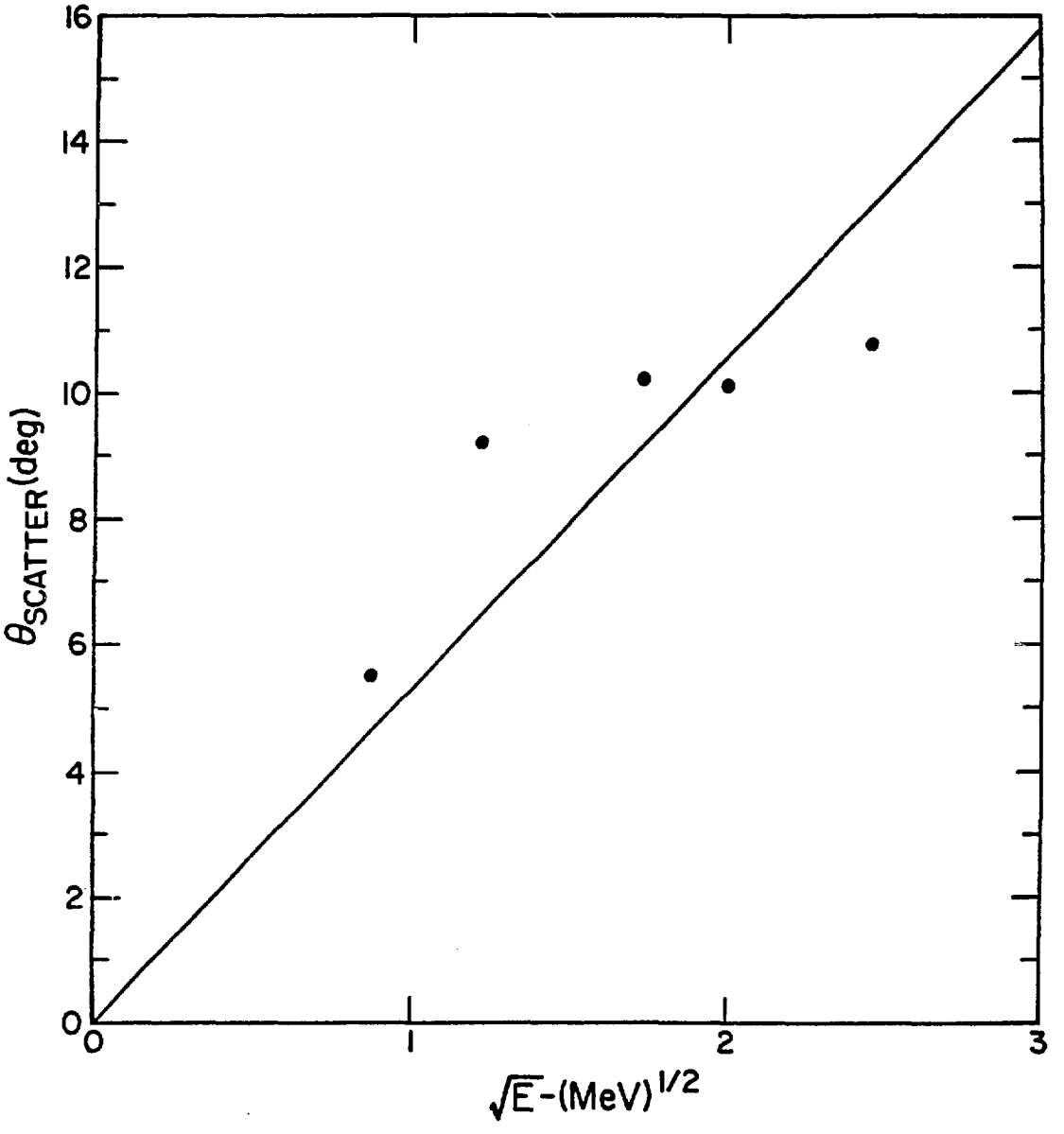

Fig. 7 Scattering angle (FWHM) defined from the difference between the squares of the observed distribution width and the calculated geometrical width, plotted vs the square root of the energy. All available angular distribution data (that is, from different channels) were used to construct this plot.

TABLE IV

GEOMETRICAL FACTOR FOR EACH CHANNEL

Channel	θ_{GEOM}
1	6.2
2	8.1
3	6.6
4	11.0

data taken at Aerospace and the University of Maryland, we replotted and shifted the curves relative to each other until we achieved a good match. Since the curves are plotted on semilogarithmic paper, such shifts correspond to multiplication by a constant in the form,

$$(\text{Aerospace end point}) = \eta^2 \, (\text{Maryland end point}).$$

The values of η for Channels 1 through 4 are 1.4, 1.4, 1.2, and 2.2. Because we do not know a priori how this renormalization should be apportioned between the two data sets, we have divided the Aerospace data sets by η and multiplied the University of Maryland data sets by η. The results of this exercise are shown in Fig. 8.

CHECK OF DEAD TIME

The BDD was checked for dead time effects on April 1, 1981 at the Rockwell International facility in Seal Beach. A BNC model DB-2 random-pulse generator stimulated the dummy head on the BDD. The pulses were shaped with a rise time of 0.2 μsec and a decay time of 20 μsec.

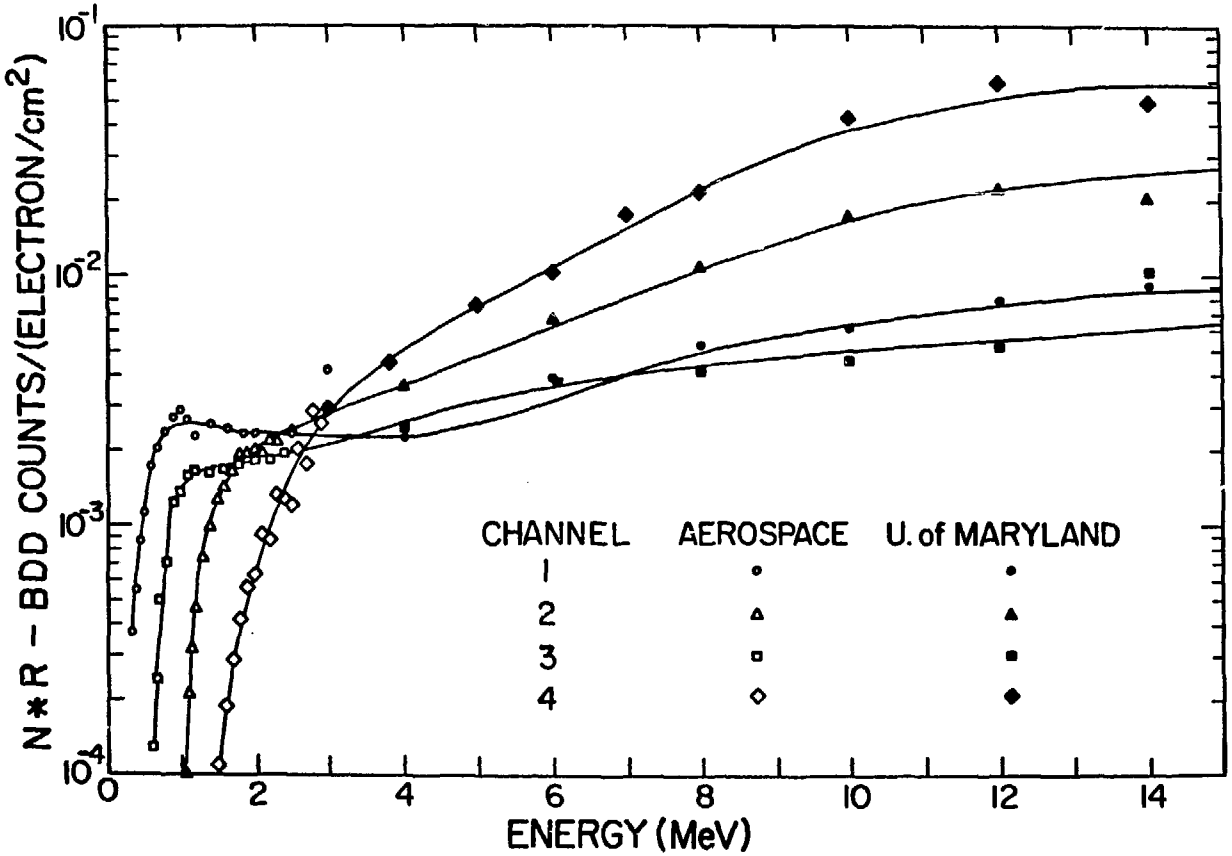

Fig. 8 Renormalized distributions for all channels. Compare these curves with those given in Fig. 3.

The upper thresholds for switching from pulses counted as electrons to those counted as protons were at 34, 26.5, 23.5, and 20.5 mV for channels 1 to 4, respectively; the thresholds for electron counts were approximately 6, 5, 5, and 4 mV, respectively.

The counting rate of the BDD instrument was measured for a number of input pulse heights at various random rates. The BDD conversion factor was chosen so that a 2-MeV energy loss in the silicon semiconductor sensors would correspond to 1 BDD count. Since 3.6-eV energy loss in silicon is required to produce one electron-hole pair, 1 BDD count is equivalent to (2 MeV ÷ 3.6 eV per pair) x (1.6×10^{-19} Coul per pair), or 8.8×10^{-14} Coulombs accumulated by the charge sensitive preamplifiers. A 1-mV test pulse deposits $1.5\text{-x-}10^{-15}$ Coulombs because our experimental arrangement used a 1.0-pF injection capacitor and our estimated stray capacitance is 0.5 pF. The tests at Rockwell were done using a fast clock so that the normal 6-min accumulation mode[1] corresponded to 24 sec. One BDD count in a 24-sec sample period thus corresponds to (8.8×10^{-14} Coul) ÷ (24-sec.), or 3.67×10^{-15} Coul/sec. This current requires (3.67×10^{-15}) ÷ (1.5×10^{-12}) or 2.45×10^{-3} pulses, one volt in magnitude, per second. Plots of the number of BDD counts per 24 seconds vs the pulser's rate multiplied by the peak amplitude for the input pulses are shown in Figs. 9 through 12. This number is a factor of 3 to 4 lower than that suggested by the data plotted in Fig. 9. These numbers are in excellent agreement with the data plotted in Fig. 9.

REDUCTION TO EQUIVALENT THRESHOLDS AND RESPONSE VALUES

A simple plane model of the filter/sensor combination predicts[1] that an effective threshold energy E^* and an effective average energy deposited in the sensor R^* can be chosen that are independent of the spectral index γ over a wide range of values. In practice isotropic fluxes and scattering effects complicate this solution, and iterative solutions are sometimes required.

Equation (1) has been numerically integrated for each of the four sensor channels, using the adjusted measured values for N*R given in Fig. 8. For $n(\theta, E)$ we assume an isotropic flux and average over θ, giving

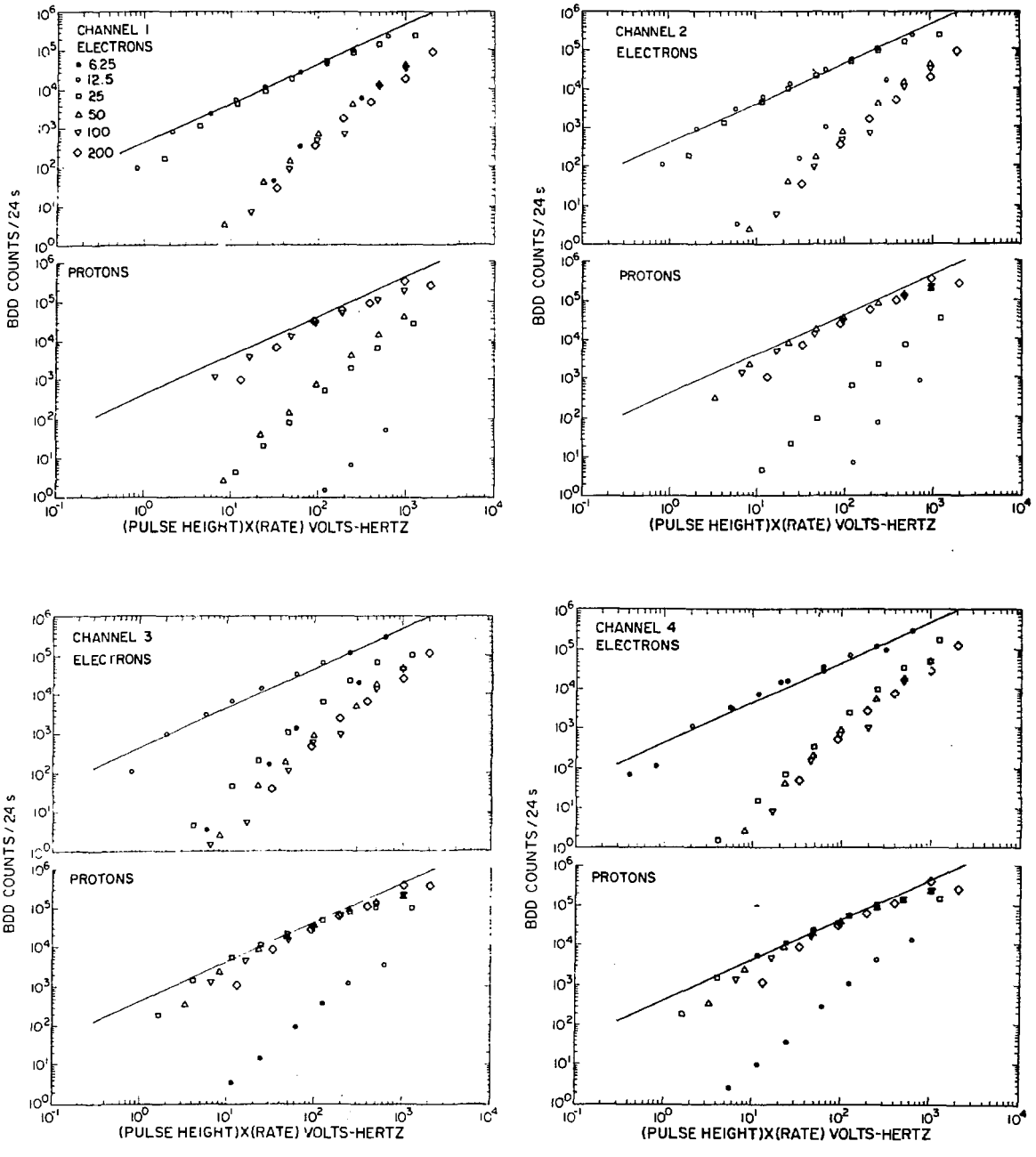

Fig. 9-12 BDD counts/(24 sec) vs Rate x Height of test pulses. These curves are analogous to a plot of observed rate vs true rate for a counter type of apparatus. The solid line is the theoretical linear relationship between BDD counts and the charge injected by the test pulser.

$$\overline{\eta(E)} = \frac{\theta_o^2}{2} = \frac{0.361}{2}\left(\theta_{GEOM}^2 + 27.8\ E\right)$$

where θ_{GEOM} is taken from Table IV and is in degrees and E is in MeV. A parametric family of curves was obtained for R^* vs E^*, with γ as the parameter. In the simple model these curves should all intersect in a common point; however, the measured sensor response functions give a skewed family of curves for each channel (Figs. 13 through 16).

From the curves in Figs. 13 through 16 one can construct new families of curves where R^* is plotted as a function of γ, with E^* being the variable parameter. Figures 17 through 20 display these constructed parametric curves for the four sensor channels. This form of display is sometimes more useful in determining the optimum values of E^* and R^* suitable for an extended range of the spectral index γ, and indeed that is the case here. We anticipate the spectral index to fall between 0.2 and 0.5 much of the time; and for these periods, we see from the above display, good average values for E^* and R^* are as given in Table V.

TABLE V

ELECTRON EQUIVALENT THRESHOLD AND RESPONSE VALUES

Channel	E^* (MeV)	R^* (MeV)
1	0.51	$1.43(10)^{-4}$ ±2%
2	0.80	$1.73(10)^{-4}$ ±5%
3	1.30	$1.29(10)^{-4}$ ±5%
4	1.75	$1.90(10)^{-4}$ ±7%

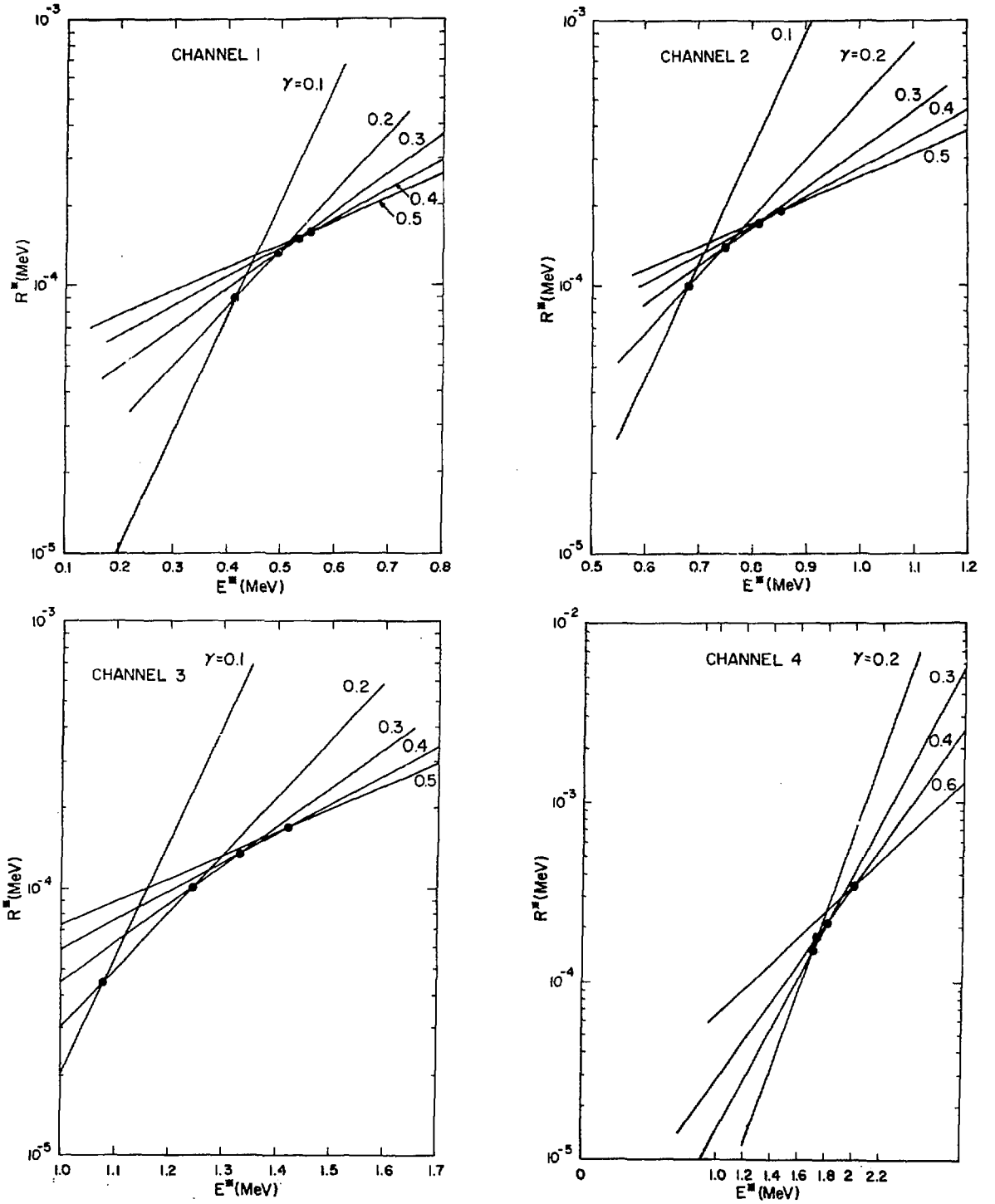

Fig. 13-16 Parametric families of curves of R^* vs E^* with the spectral index, γ, as a variable parameter, for Channels 1 through 4, respectively. These were calculated from the adjusted measured values for N*R given in Fig. 8.

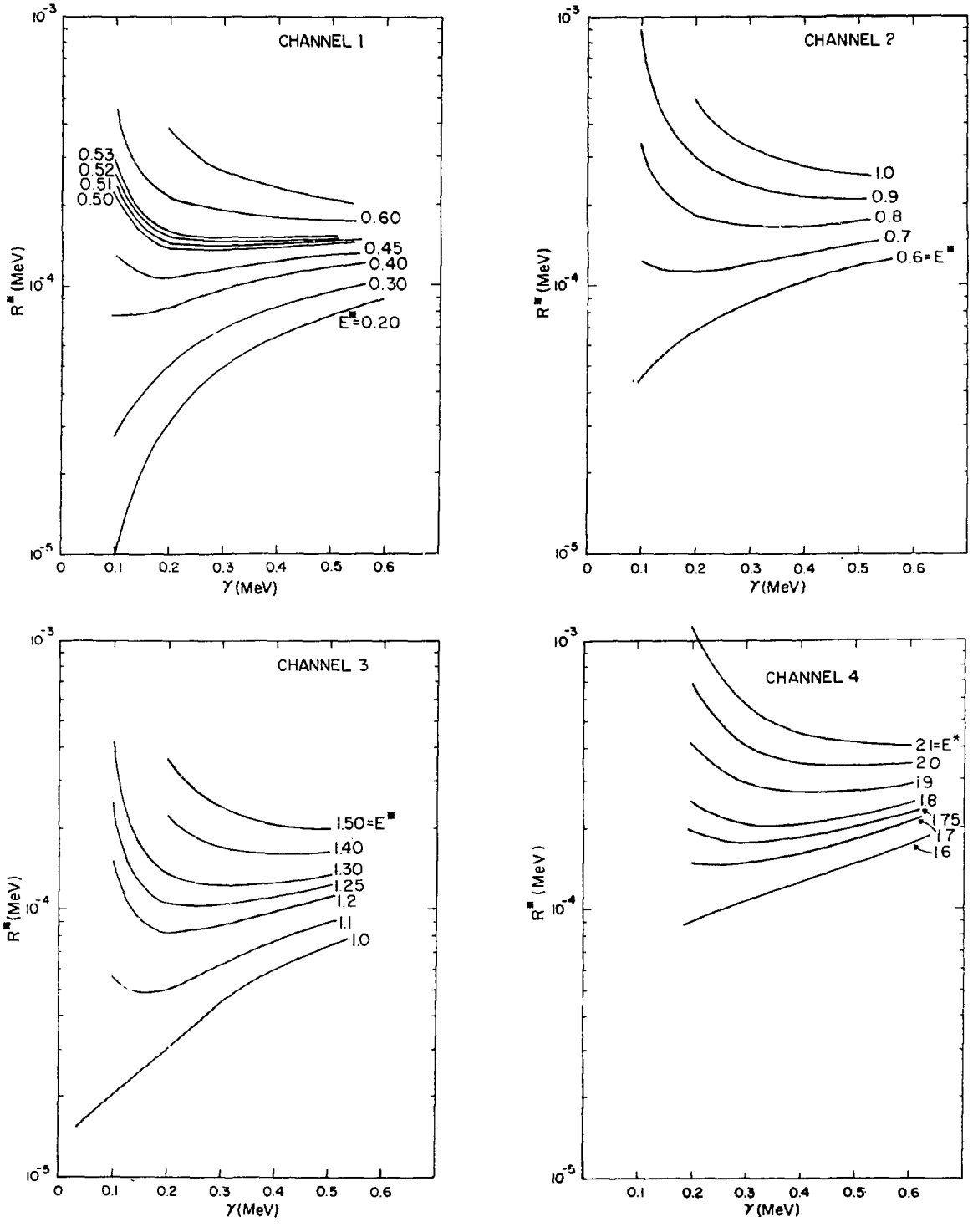

Fig. 17-20 Parametric families of curves of R^* vs γ, with E^* being the variable parameter, for Channels 1 through 4, respectively. These have been constructed from the families of curves in Fig. 13 through 16. Compare with Table V.

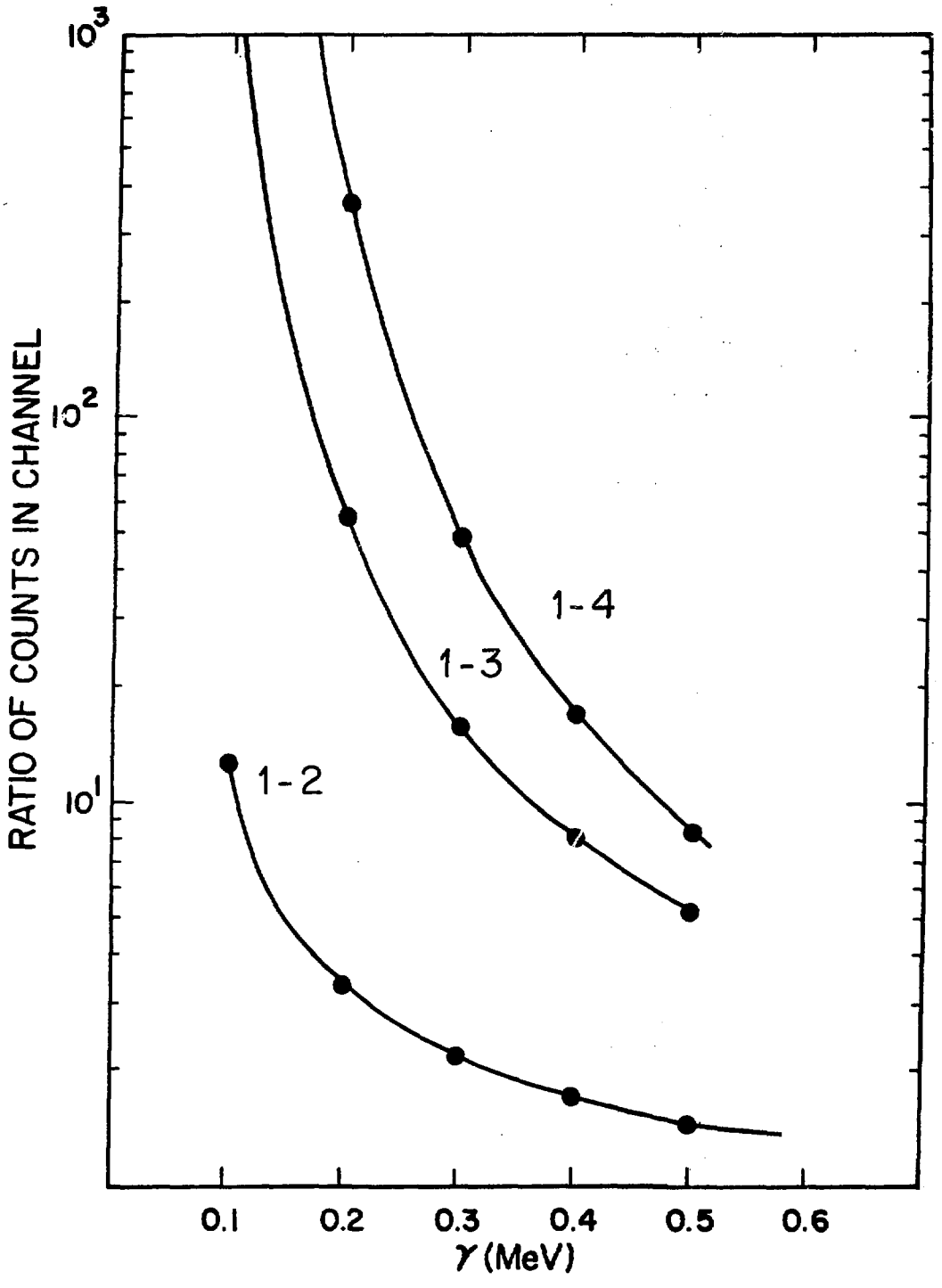

Fig. 21 The ratios of counts observed in each of the four channels plotted as functions of the spectral index, γ.

The numerical integration of Eq. (1), as discussed above for each of the four channels with γ as the parameter, has provided us with ratios of counts to be expected when comparing any two channels. The ratios of Channels 1/2, 1/3, and 1/4 have been plotted in Fig. 21 as a function of the spectral index γ.

Preliminary data analysis consists of comparing the observed ratios of channel counts with the curves of Fig. 21 and selecting the best γ fit. If it falls between 0.2 and 0.5, Table V gives the appropriate E^* and R^* to use.

For each channel, dividing the observed counts by the appropriate R^* gives the number of electrons per cm^2, omni-directional, of energy greater than E^*. The four channels will give four points on this integral flux curve, together with the spectral index.

ACKNOWLEDGMENTS

We thank B. Blake, J. Fennel, and S. Immamoto at The Aerospace Corporation; W. Chappis and R. Starrett at the University of Maryland; and G. Lockwood and L. Ruggles at Sandia Laboratories, Albuquerque for their help and hospitality during these calibrations. We also thank the many technicians at the Los Alamos National Laboratory who helped make these efforts successful; in particular, R. Cope, D. Deck, and W. Everett. Our special thanks go to J. Hartmann who shared with us the late hours and weeks of travel to the East and West Coasts.

REFERENCES

1. H. V. Argo, D. N. Baker, R. D. Belian, L. K. Cope, and P. R. Higbie, The BDD: A Dosimeter for the Global Positioning System, Los Alamos National Laboratory report LA-8421-MS (October 1980).

2. J. D. Sullivan, Geometric Factor and Directional Response of Single and Multi-Element Particle Telescopes, Nucl. Instrum. & Methods, 95, 5 (1971).